Strengthening of perforated walls in cable-stayed bridge pylons with double cable planes

Bin Cheng [1,3], Jie Wu [*2] and Jianlei Wang [1]

[1] *Department of Civil Engineering, Shanghai Jiao Tong University, Shanghai 200240, China*
[2] *College of Civil Engineering, Tongji University, Shanghai 200092, China*
[3] *State Key Laboratory of Ocean Engineering, Shanghai Jiao Tong University, Shanghai 200240, China*

Abstract. This paper focuses on the strengthening methods used for improving the compression behaviors of perforated box-section walls as provided in the anchorage zones of steel pylons. Rectangular plates containing double-row continuous elliptical holes are investigated by employing the boundary condition of simple supporting on four edges in the out-of-plane direction of plate. Two types of strengthening stiffeners, named flat stiffener (FS) and longitudinal stiffener (LS), are considered. Uniaxial compression tests are first conducted for 18 specimens, of which 5 are unstrengthened plates and 13 are strengthened plates. The mechanical behaviors such as stress concentration, out-of-plane deformation, failure pattern, and elasto-plastic ultimate strength are experimentally investigated. Finite element (FE) models are also developed to predict the ultimate strengths of plates with various dimensions. The results of FE analysis are validated by test data. The influences of non-dimensional parameters including plate aspect ratio, hole spacing, hole width, stiffener slenderness ratio, as well as stiffener thickness on the ultimate strengths are illustrated on the basis of numerous parametric studies. Comparison of strengthening efficiency shows that the continuous longitudinal stiffener is the best strengthening method for such perforated plates. The simplified formulas used for estimating the compression strengths of strengthened plates are finally proposed.

Keywords: steel pylon; double cable planes; perforated plate; elliptical hole; strengthening method; uniaxial compression

1. Introduction

In box-section steel pylons of cable-stayed bridges where double cable planes are commonly adopted, cutouts in the outer walls are inevitable in the anchorage zones to hold the cables. The openings are usually of elliptic shapes arising from the oblique angles between the cables and the pylon, and two rows of multiple holes are often continuously provided corresponding to the number of cables and the anchorage locations, as shown in Fig. 1. No out-of-plane loading occurs to the perforated plates through which the cables run, because the gaps between the cables and the hole edges are always reserved for deforming. Instead, due to the collaboration of sectional walls,

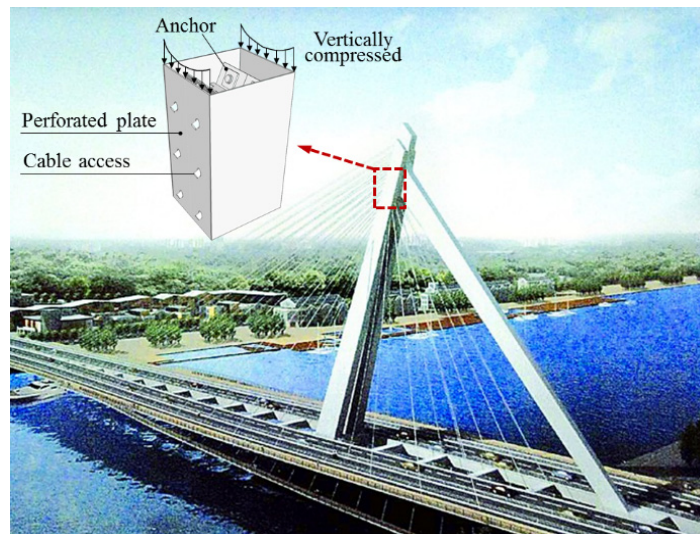∗Corresponding author, Ph.D., E-mail: wwujie@tongji.edu.cn

Fig. 1 Perforated plates containing double-row continuous elliptical holes in the cable anchorage of a steel tower

the perforated plates are uniaxially compressed in the in-plane direction despite that the cables are anchored onto the other non-perforated plates perpendicular to the perforated ones, and evidently, the lower plates bear higher compressive stresses than the upper plates. These perforated plates, commonly act as flanges of a box section, are more prone to compressive failure than those non-perforated web plates for the following reasons: (1) additional compressive stresses caused by significant sectional moments of the tower in the longitudinal plane of the bridge may occur on the flanges (i.e., perforated plates); (2) sectional areas of the plates are remarkably reduced because of the holes; and (3) the out-of-plane rigidity of the non-perforated web plates are improved since they are laterally connected with and thus supported by the rigid anchor systems.

The presence of continuous holes in such structures is expected to result in a significant increase in stress concentration and a remarkable reduction in ultimate bearing capacity of the compressed plate when compared to the non-perforated one. If the degraded ultimate strength of the perforated plate fails to meet the requirement of structural safety, an appropriate cutout-strengthening method should be adopted to improve the behaviors. Unfortunately, there is no usable reference in existing literatures including current design codes for the strengthening of such holes.

The studies on the stress concentrations of perforated plates were firstly carried out for infinite plates by Muskhelishvili (1963), Savin (1961), and Peterson (1974), followed by the work concerning finite plates conducted by She and Guo (2007), Yang *et al*. (2008), Li *et al*. (2008), and Yu *et al*. (2008). More efforts were devoted to the ultimate strengths by considering the elasto-plastic buckling of the plate. Narayanan and Rockey (1981) carried out the ultimate strength tests on thin-walled webs containing a circular hole and presented a method to approximately predict the ultimate capacity of plate girders with perforated webs. Azizian and Roberts (1983) performed the geometrically nonlinear elasto-plastic analysis using finite element method for axially compressed square plates with centrally placed square and circular holes. Narayanan and Chow (1984) presented an approximate method of predicting the ultimate load carrying capacity of

simply supported perforated plates under uniaxial compression, whose reliability was validated by comparing with test results. Curves suitable for the use of designers have also been proposed in their study to determine the ultimate capacity of square plates with centrally placed holes. Shanmugam *et al.* (1999) proposed a design formula, on the basis of the results from the finite element analyses, to determine the ultimate load carrying capacity of perforated square plates with square or circular holes for the cases of different boundary conditions and uniaxial or biaxial compression. El-Sawy *et al.* (2004) focused on the elasto-plastic buckling of uniaxially loaded square and rectangular plates with circular cutouts by the use of the finite element method, including some recommendations about hole size and location for the perforated plates of different aspect ratios and slenderness ratios. Paik (2007a, b, 2008) investigated the ultimate strength characteristics of perforated plates under edge shear loading, axial compressive loading and the combined biaxial compression and edge shear loads, and proposed closed-form empirical formulae for predicting the ultimate strength of perforated plates based on the regression analysis of the nonlinear finite element analyses results. Maiorana *et al.* (2008, 2009) performed the linear and nonlinear finite element analyses of perforated plates subjected to localized symmetrical load. Moen and Schafer (2009) described the elastic buckling behaviors and proposed closed-form expressions for critical elastic buckling stresses of plates with single or multiple perforations including slotted holes under bending and compression. Cheng *et al.* (2013a, b) experimentally and numerically investigated the influences of slotted holes and continuous elliptical holes on the stress concentrations and ultimate strengths of the compressed plates in steel pylons, with enclosed formulae having been proposed for the strength estimation. Cheng and Zhao (2010) and Cheng and Li (2012) also investigated the cutout-strengthening of uniaxially compressed and shear loaded square plates containing single circular hole by the use of finite element method. In summary, behaviors of perforated plates considering various parameters have been comprehensively investigated in previous researches, and some recommendations and formulas beneficial for practical engineering design have also been presented. However, none of them are related to the strengthening of double-row continuous elliptical holes.

As a continued work for the authors' previous research (Cheng *et al.* 2013a), this research further focuses on the strengthening methods as used to improve the compression behaviors of plates perforated by double-row continuous elliptical holes. The studied plates are supposed to be simply supported in the out-of-plane direction on their four edges. The two rows of elliptical holes are symmetrically located about the center line of the plate, and uniaxial in-plane compression is considered according to the practical stress distribution of plates in pylon. Two types of strengthening stiffeners, i.e., flat stiffener (FS) and longitudinal stiffener (LS), are considered. Compression test of both unstrengthened and strengthened plates is carried out by the use of a self-balanced loading device, followed by a large number of parametric numerical studies concerning various dimensions of plates, holes, and stiffeners using finite element method. Behaviors such as stress concentrations, out-of-plane deformations, failure patterns as well as elasto-plastic ultimate strengths of the plates are investigated. The influences of non-dimensional parameters including plate aspect ratio, hole spacing, hole width, stiffener slenderness ratio, as well as stiffener thickness on the ultimate strengths are obtained. Comparisons in strengthening efficiencies of stiffeners are also made, and the simplified formulas used for estimating the compression strengths of strengthened plates are finally proposed for engineering applications.
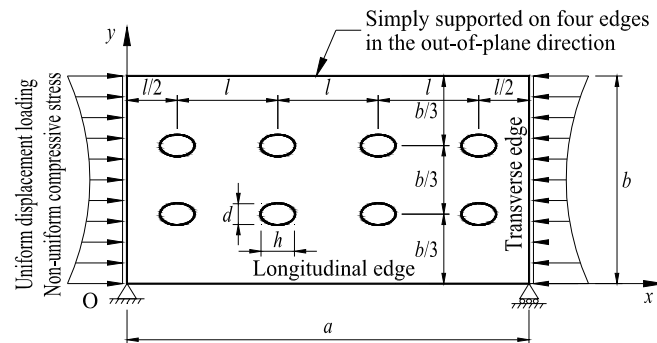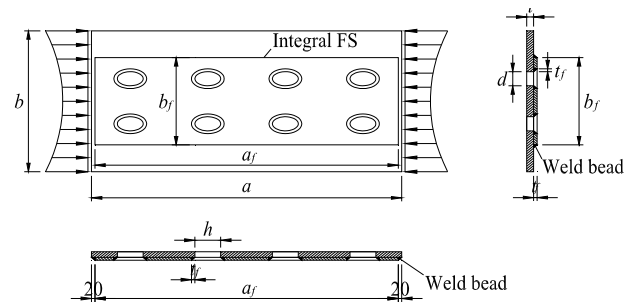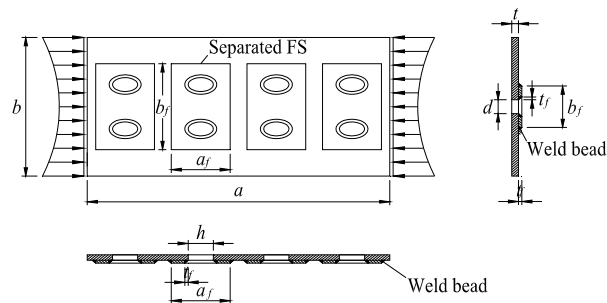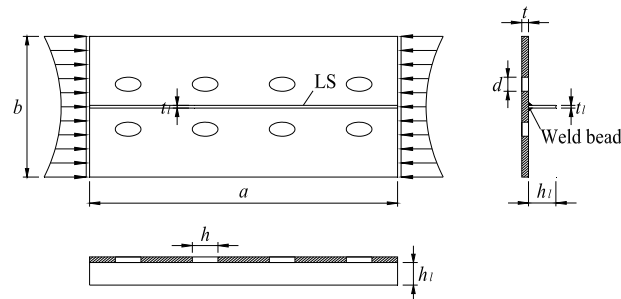

2. Test setup

Fig. 2 The unstrengthened perforated plate containing double-row continuous elliptical holes

(a) Integral FS-strengthened

(b) Separated FS-strengthened

(c) LS-strengthened

Fig. 3 The strengthened perforated plate containing double-row continuous elliptical holes

2.1 Test specimens

Totally 18 perforated rectangular plates were fabricated, of which 5 were unstrengthened plates, 13 were strengthened plates.

For the unstrengthened (UN) plates perforated by continuous elliptical holes, three non-dimensional parameters, that is, plate aspect ratio a/b, hole width/plate width d/b, and hole spacing/length l/h, were mainly considered, and the selected values were $a/b=1.8$, $d/b=0.1$ and 0.2, $l/h=2$, 3 and 4, respectively. Here, a, b, d, h, and l correspond to the plate length, width, and the hole width, length, spacing, respectively (Fig. 2). The plate slenderness ratios, i.e., b/t, of all specimens were selected as 30, a value commonly adopted in real structures so that the local buckling of steel plates could be prohibited. Two rows of holes are symmetrically located at the one-third line of plate's transverse edge. As a result of the oblique angles between the stayed cables and the pylon, the length of elliptical hole was always selected as 1.5 times its width, that is, $h/d=1.5$.

For the strengthened plates, two types of strengthening stiffeners named flat stiffener (FS) and longitudinal stiffener (LS), as shown in Fig. 3, were investigated.

(1) For the FS-strengthened plate, three fabricating steps were adopted. Firstly, two rows of continuous elliptical holes each with width of $(d + 2t_f)$ and length of $(h + 2t_f)$ were perforated in the rectangular flat stiffener with length of a_f, width of b_f, and thickness of t_f, with the hole spacings equal to those of holes provided in the compressed plate. The

Table 1 Structural parameters of specimens

Specimen	Dimensional parameter(mm)												Non-dimensional parameter					
	a	b	t	d	h	n	l	t_f or t_l	a_f	b_f	h_l	δ_0	b/t	a/b	d/b	l/h	t_f/t or t_l/t	δ_0/b
DEH1-UN	432	240	8	24	36	6	72	N/A	N/A	N/A	N/A	2.70	30	1.8	0.1	2	N/A	0.0113
DEH1-FS05								4	422	136	N/A	0.63					0.5	0.0026
DEH1-LS05								4	N/A	N/A	40	1.2					0.5	0.0050
DEH2-UN	432	240	8	24	36	4	108	N/A	N/A	N/A	N/A	1.55	30	1.8	0.1	3	N/A	0.0065
DEH2-FS05								4	404	136	N/A	1.35					0.5	0.0056
DEH2-FS05'								4	80	136	N/A	1.45					0.5	0.0060
DEH2-LS05								4	N/A	N/A	40	1.23					0.5	0.0051
DEH3-UN	432	240	8	24	36	3	144	N/A	N/A	N/A	N/A	0.65	30	1.8	0.1	4	N/A	0.0027
DEH3-FS05								4	368	136	N/A	0.9					0.5	0.0038
DEH3-FS05'								4	80	136	N/A	1.75					0.5	0.0073
DEH3-LS05								4	N/A	N/A	40	0.15					0.5	0.0006
DEH4-UN	432	240	8	48	72	3	144	N/A	N/A	N/A	N/A	0.28	30	1.8	0.2	2	N/A	0.0012
DEH4-FS05								4	422	184	N/A	0.55					0.5	0.0023
DEH4-LS05								4	N/A	N/A	40	0.33					0.5	0.0014
DEH5-UN	432	240	8	48	72	2	216	N/A	N/A	N/A	N/A	2.10	30	1.8	0.2	3	N/A	0.0088
DEH5-FS05								4	368	184	N/A	0.5					0.5	0.0021
DEH5-FS05'								4	152	184	N/A	0.63					0.5	0.0026
DEH5-LS05								4	N/A	N/A	40	1.3					0.5	0.0054

perforated stiffener, then, was tightly attached to the surface of the plate to be strengthened, with elliptical holes in the plate and the stiffener being concentric. The welding was finally carried out along the inner (hole) edge and the four outer edges of the flat stiffener. Besides the integrated stiffener (i.e., one stiffener for all holes), separated stiffeners, i.e., one stiffener for two holes, were also considered for the purpose of comparison.

(2) For the LS-strengthened plate, a stiffener with thickness of t_l and width of h_l were welded to the perforated plate so that they were perpendicular to the plate plane and parallel to the load direction (i.e., longitudinal direction). The stiffener was located at the center line of the plate.

The structural parameters of specimens are given in Table 1. All plates were identical in width and thickness but varying in length. Approximate half-wave sinusoidal distributions of initial shapes in the out-of-plane direction were observed for the plates, and the measured maximal initial deflections (δ_0) are also listed in Table 1.

Twelve standard samples taken from the 8mm and 4mm thick steel plates, six from each, were tested in uniaxial tension, and the average measured mechanical properties are given in Table 2.

2.2 Test rig

Table 2 Mechanical properties of steel

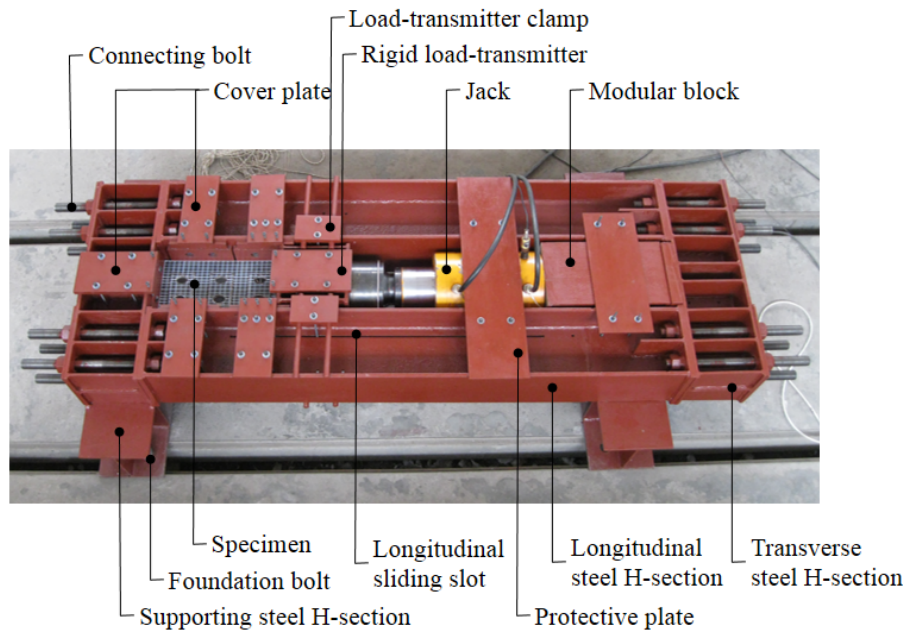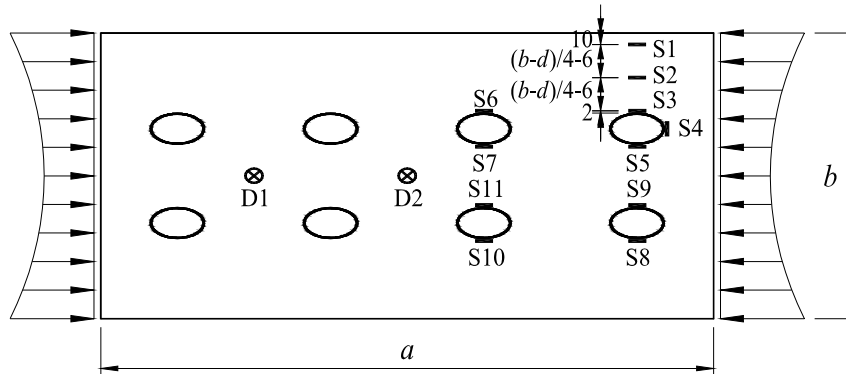| Thickness (mm)	Yield stress S_y (MPa)	Ultimate stress S_u (MPa)	Modulus of elasticity E (GPa)
8	229	366	206
4	265	402	215

Fig. 4 Overall picture of test rig

Fig. 5 Locations of strain gauges and displacement meters

As has been discussed in the authors' pervious work (Cheng *et al*. 2013a), the boundary constraints of simple support in the out-of-plane direction of plate's four edges and the load conditions of uniform-displacement/nonuniform-stress compression on plate's transverse edges, as shown in Fig. 2, were adopted in this research, so that the specimens are as real as those in practical structures. The test rig is therefore expected to not only provide simple and rotatable supports along four edges of the specimen but provide a convenient mechanism to apply uniform or rigid compressive displacements on the transverse edges of the plate. Moreover, flexibility to accommodate the plates with various lengths is also required for the rig. A self-balanced loading device, as shown in Fig. 4, was designed to meet the requirements. More details of the test rig have been introduced by Cheng *et al*. (2013a).

2.3 Measurements

The arrangement of strain gauges were shown in Fig. 5, in which S1, S2, and S3 were used to reveal the elastic stress distribution along the middle transverse section of the specimen. The rest of the strain gauges (S4 to S11) were assigned to the potential locations where high compression/tension stresses have been verified from the previously conducted finite element analysis.

Two displacement meters D1 and D2 were also placed near the mid span and quarter span of the plate to record the out-of-plane deformations, as shown in Fig. 5.

3. Test results

3.1 Stress concentrations

It has been reported in the authors' previous work that the outer endpoint of the minor axis of the elliptical hole that is closest to the loaded transverse edges always gave the maximal compressive stress of a perforated plate containing double-row continuous elliptical holes (Cheng *et al*. 2013a). Therefore, the influences of strengthening stiffener on stress level at gauges S3 and S8 were mainly focused on in this paper. Fig. 6 typically shows the load versus S3 strain curves of series DEH5 specimens, as obtained from the first several loading steps (i.e., elastic stage). It can
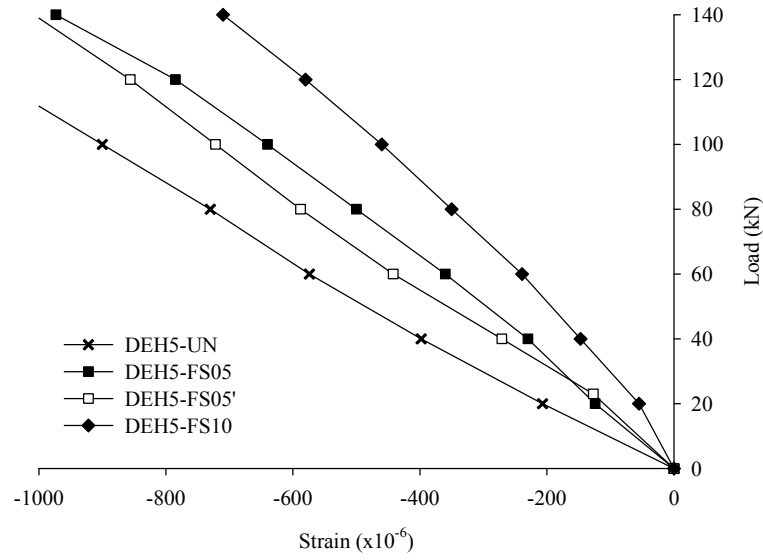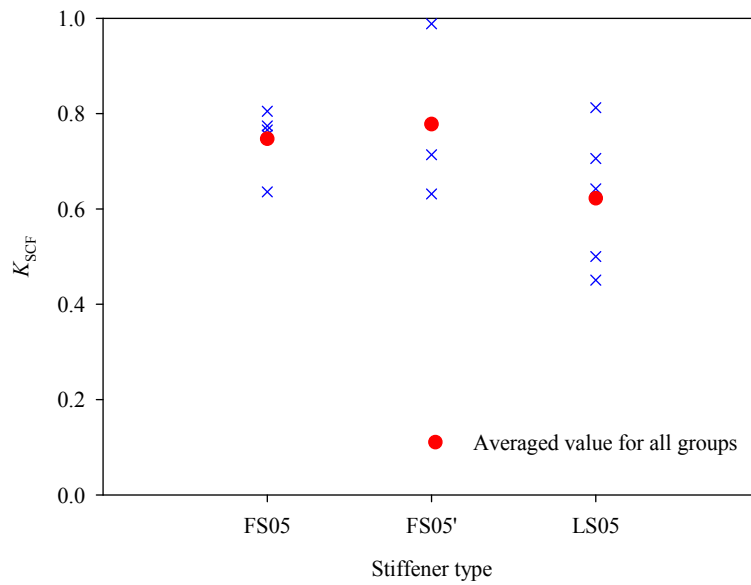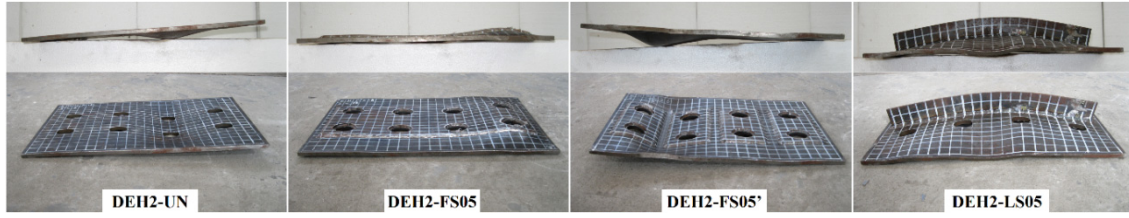
Fig. 6 Load vs S3 strain curves of series DEH5 specimens

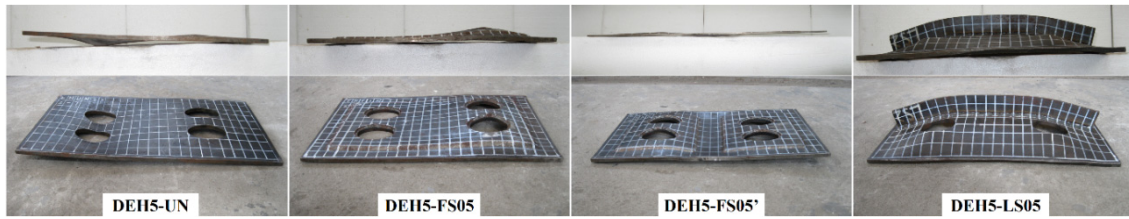Fig. 7 SCF reduction factors (K_{SCF}) for various stiffeners

be seen that, compared to unstrengthened plate, the compressive strains of strengthened plates were more or less depressed by the stiffeners.

In order to quantify the influence, SCF reduction factor (K_{SCF}) was further introduced as

$$K_{SCF} = \frac{\text{SCF of strengthened plate}}{\text{SCF of unstrengthened plate}}$$

(a) Series DEH2

(b) Series DEH4

Fig. 8 Typical failure patterns of specimens

where SCF is calculated as

$$SCF = \frac{Longitudinal\ stress\ at\ gauge\ S3}{Averaged\ longitudinal\ stress\ on\ the\ transverse\ edge}$$

Fig. 7 shows the K_{SCF} of all specimens, as categorized by stiffener type. It can be found that the differences in averaged K_{SCF} between integral FS-strengthened and separated FS-strengthened plates are invisible. The longitudinal stiffeners could be more efficient in reducing the stress concentrations since the corresponding K_{SCF} values are slightly lower than others.

3.2 Failure patterns

Fig. 8 shows the typical failure patterns of the tested plates, with elevation views and aerial views being both demonstrated. Local buckling of steels near the hole edge were commonly observed for unstrengthened and FS-strengthened plates, which means flat stiffeners can hardly change the failure modes. Moreover, the steels between adjacent flat stiffeners of separated FS-strengthened plates are also prone to local buckling, see specimen EH12-FS05'. The LS-strengthened plates were always found to be compressed to failure according to overall buckling mode, that is, the out-of-plane deformations in both orthotropic directions followed approximate half-wave sinusoidal distributions. A plausible explanation is that the longitudinal stiffeners provided considerable evenly distributed lateral stiffness for the plate, which prevented the steels from deforming and buckling locally.

3.3 Ultimate strengths

3.3.1 Case of different hole size
For the purpose of comparison, strength improvement factor (R_s) was introduced as

$$R_s = \frac{\text{Ultimate strength } (P_{ult}) \text{ of strengthened plate}}{\text{Ultimate strength } (P_{ult}) \text{ of unstrengthened plate}}$$

Experimental R_s of three strengthening methods are plotted in Fig. 9, as categorized by the hole size. It is evident that the strengthening effect becomes better for larger holes since R_s of strengthened plates with $d / b = 0.2$ are greater than those of specimens with $d / b = 0.1$. The conclusion is further confirmed by comprehensive finite element analysis that will be presented next, as shown in Fig. 18.

3.3.2 Case of different stiffener type

Fig. 10 shows the comparison of ultimate strengths for the plates strengthened by different stiffeners. It can be found that

(1)   The strength improvements of integral FS-strengthened plates for the comparing series DEH3 and DEH5 are respectively 24%, and 15% higher than those of separated FS-strengthened plates, which indicates that integral flat stiffener is more effective in enhancing the bearing capacities. The buckling of unstrengthened steels between separated flat stiffeners, as have been observed during the testing, are regarded by the authors as the real causes of the earlier failure. Therefore, integral flat sitffener instead of separated multiple flat stiffeners is suggested for the engineering applications and thus mainly focused on in this research.

(2)   In case of identical stiffener thickness, integral flat stiffener leads to 6-24% higher strength improvement than longitudinal stiffener for the same unstrengthened plate. This could be
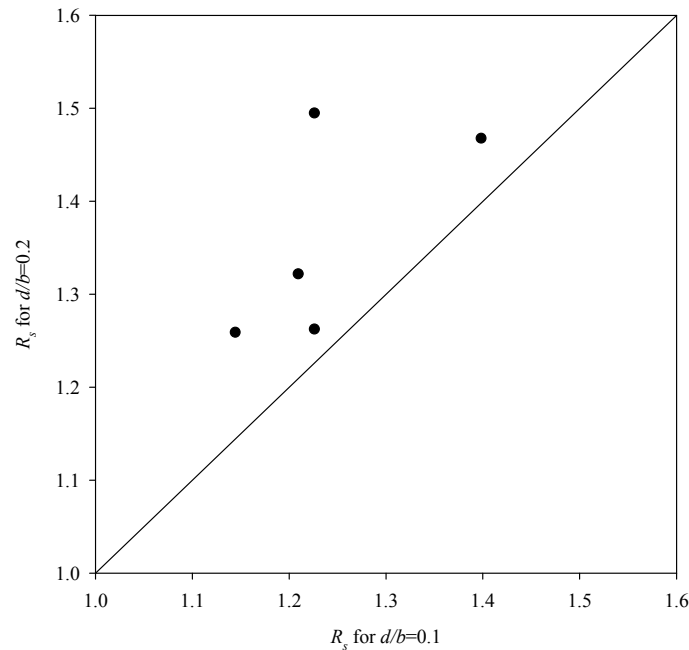

Fig. 9 Comparison of strength improvements for the plates with different hole sizes
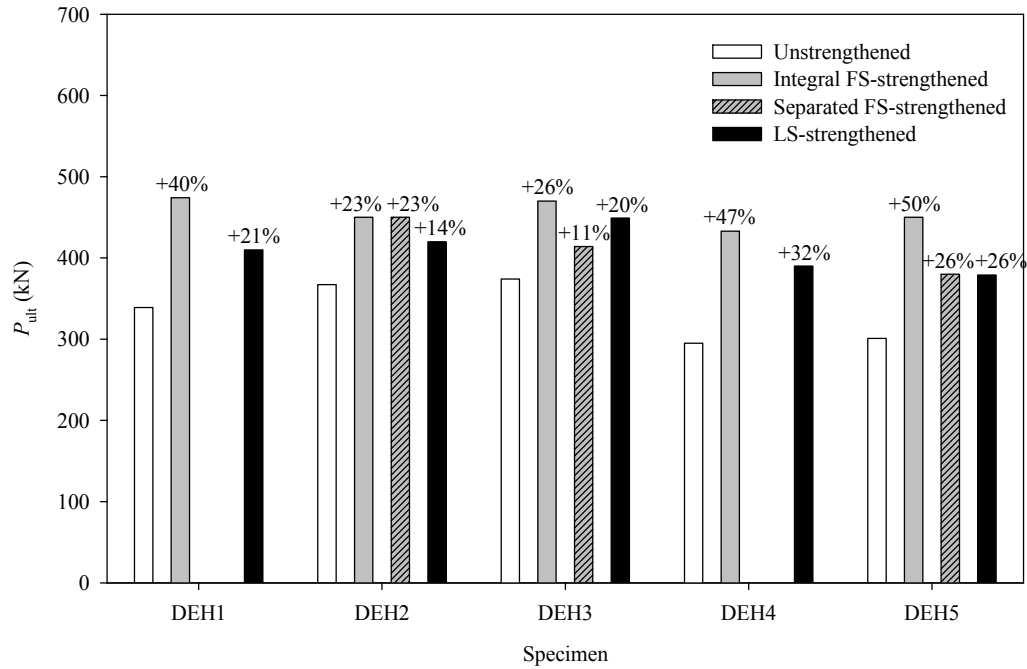
Fig. 10 Comparison of strengths for the plates strengthened by different stiffeners

Table 3 Experimental elastic SCFs, ultimate strengths S_{ult}, and ultimate out-of-plane displacements δ_{max}

Specimen	SCF	K_{SCF}	P_{ult} (kN)	S_{ult} (MPa)	S_{ult}/S_y	R_s	δ_{max} (mm)	δ_{max}/b	Longitudinal location of δ_{max}
DEH1-UN	3.84	1	339	176.56	0.771	1	16.7	0.0696	One-third span
DEH1-FS05	3.09	0.80	474	246.88	1.078	1.40	17.0	0.0708	Quarter span
DEH1-LS05	1.73	0.45	410	213.54	0.932	1.21	25.3	0.1054	Mid span
DEH2-UN	3.23	1	367	191.15	0.835	1	17.4	0.0725	One-third span
DEH2-FS05	2.50	0.77	450	234.38	1.023	1.23	11.0	0.0458	Near transverse edge
DEH2-FS05'	2.04	0.63	450	234.38	1.023	1.23	21.0	0.0875	Quarter span
DEH2-LS05	2.28	0.71	420	218.75	0.955	1.14	18.0	0.0750	Mid span
DEH3-UN	2.56	1	374	194.79	0.851	1	22.5	0.0938	Mid span
DEH3-FS05	1.96	0.77	470	244.79	1.069	1.26	20.8	0.0867	Near transverse edge
DEH3-FS05'	2.53	0.99	414	215.63	0.942	1.11	12.5	0.0521	Quarter span
DEH3-LS05	2.08	0.81	449	233.85	1.021	1.20	28.2	0.1175	Mid span
DEH4-UN	4.08	1	295	153.65	0.671	1	22.7	0.0946	Mid span
DEH4-FS05	3.08	0.75	433	225.52	0.985	1.47	15.7	0.0654	Quarter span
DEH4-LS05	2.62	0.64	390	203.13	0.887	1.32	29.5	0.1229	Mid span
DEH5-UN	3.98	1	301	156.77	0.685	1	25.6	0.1067	Quarter span
DEH5-FS05	2.53	0.64	450	234.38	1.023	1.50	21.2	0.0883	Quarter span
DEH5-FS05'	2.84	0.71	380	197.92	0.864	1.26	8.5	0.0354	Mid span & Quarter span
DEH5-LS05	1.99	0.50	379	197.40	0.862	1.26	34.3	0.1429	Quarter span

attributed to: (1) the longitudinal stiffener is located far away from the hole edges ; and (2) the longitudinal stiffener only affect the local areas near the center line of the plate, while the flat stiffeners cover most of the plate's transverse section.

The experimental results are summarized in Table 3.

4. Numerical analysis

4.1 Finite element model

A general-purpose finite element program ANSYS (2009) was used to obtain the elasto-plastic ultimate strengths (P_{ult}) of unstrengthened and strengthened perforated plates. In the analysis, the applied displacements at plate's transverse edges were gradually increased until the collapse happened, and the von Mises yield criterion was employed to determine the structural failure.

The tested material properties of steel were applied to all finite element models (FEM). A multilinear isotropic hardening stress-strain curve corresponding to the experimental results of steel samples was assigned to the specimens during the FEM validation analysis. While for the numerous parametric analyses of plates with various dimensions, the steel material was assumed to be linearly elastic before yielding and perfectly plastic after yielding (i.e. with no stain hardening). Fig. 11 demonstrates both experimental and FE used stress-strain relationship curves, where S_y and S_u respectively represents the experimental yield stress and ultimate stress of the steel, and ε_y and ε_u correspond to the experimental strains at yield point and ultimate point. Moreover, ε_h in the figure is the experimental strain from which the steel begins hardening. The initial geometric imperfections followed the half-wave sinusoidal mode as observed from the specimens, and the initial deflection amplitudes were chosen to be the measured values (δ_0) for validation analysis and $b/1000$ for parametric analysis, respectively.
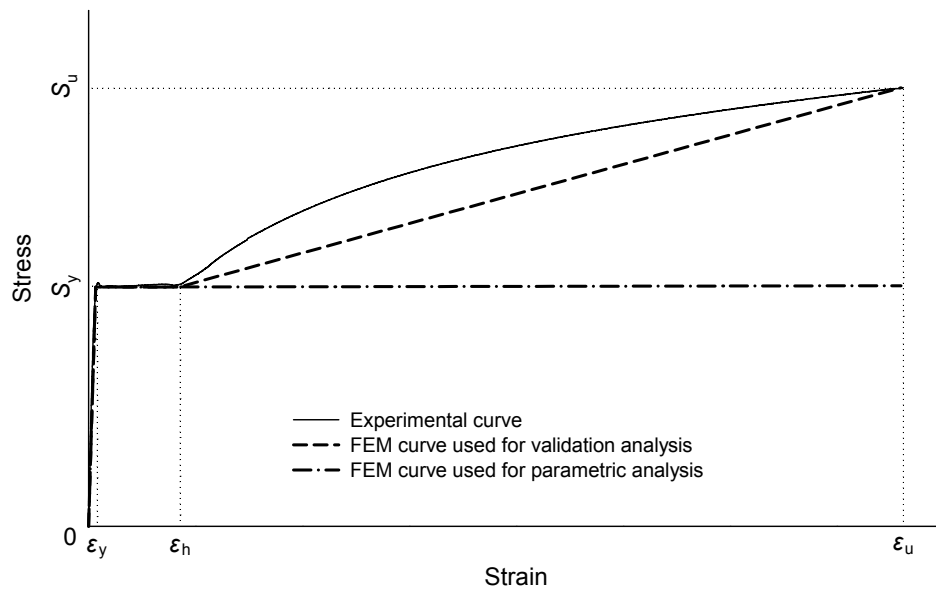

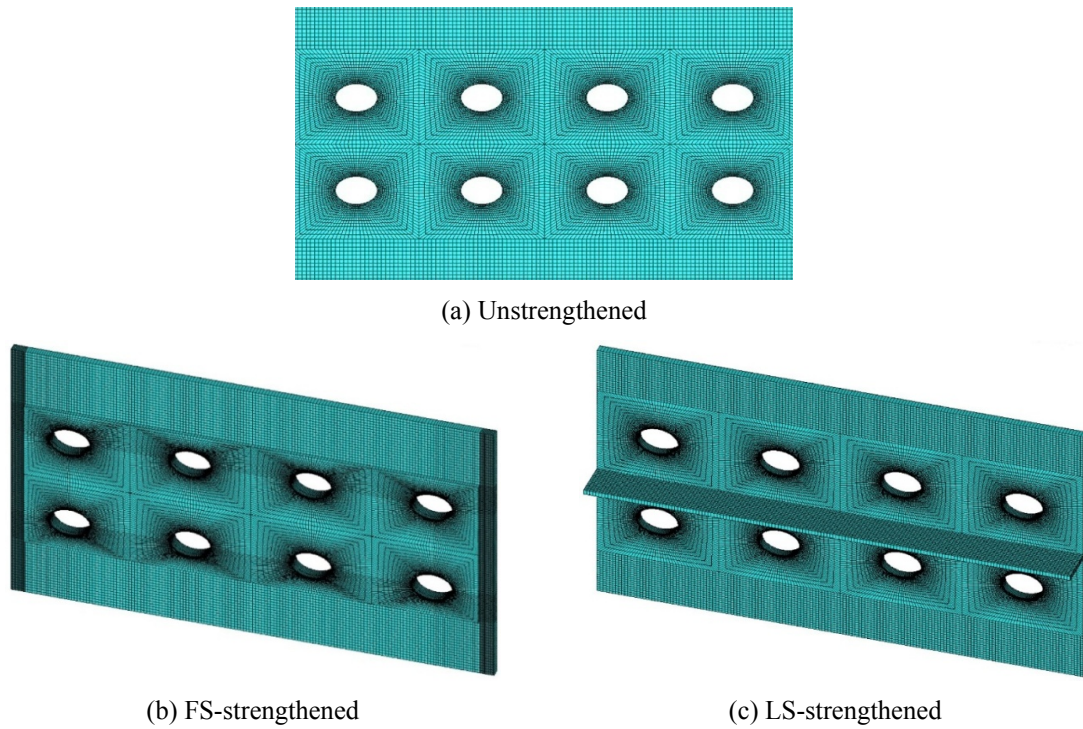Fig. 11 Stress-strain relationship curves of steel

(a) Unstrengthened

(b) FS-strengthened

(c) LS-strengthened

Fig. 12 Finite element meshes of perforated plate with $a/b=2.0$ and $d/b=0.1$, with double rows of holes

(a) Load case I for continuous LS
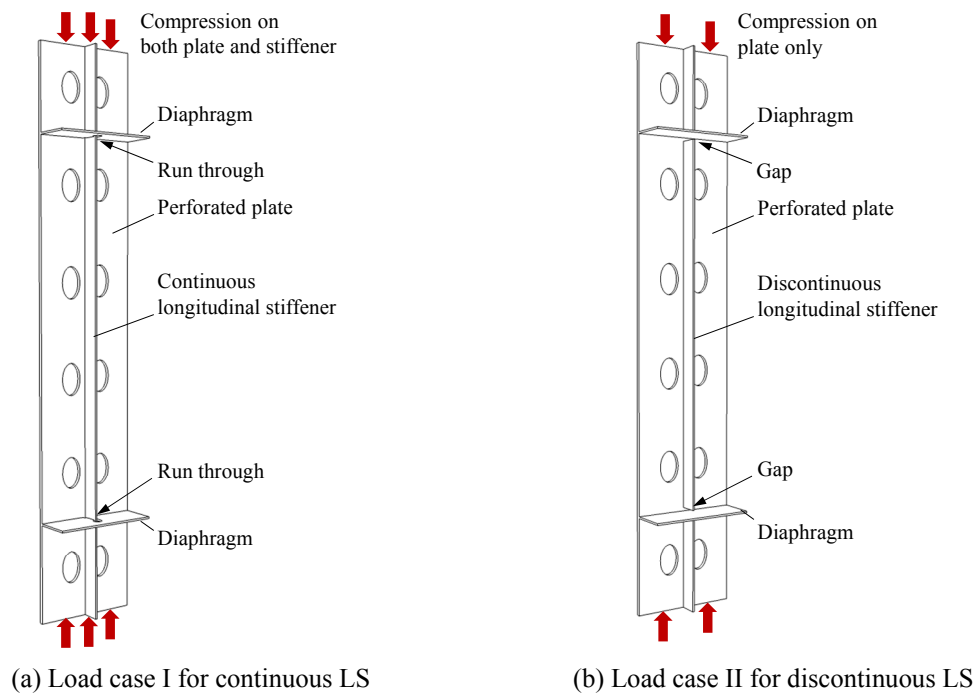

(b) Load case II for discontinuous LS

Fig. 13 Load cases of LS-strengthened plates

Plate elements (SHELL181) with four nodes and six degrees of freedom for each node were used in the present research, with the influence of transverse shear deformation having been considered (ANSYS 2009). The meshes around the elliptical holes were subdivided to take into account the complexity of stress distribution inside these zones. The element sizes along the plate edges and the hole edges were $b_f/40$ and $(\pi+1)d/160$, respectively, indicating that the element size gradually increased by approximately triple from the hole edge to the plate edges. For the strengthened plates, the average element size on the longitudinal and transverse edges of the flat stiffener is $a_f/(40n)$ and $b_f/40$, respectively, and the average element size in the longitudinal stiffener is $(\pi d)/160$. Typical finite element meshes are demonstrated in Fig. 12.

For the LS-strengthened plates, two load cases are separately considered in the parametric analysis:

Case I – The uniform compressive displacements were applied on both the plate and the stiffeners, which is consistent with the compression test conducted. This case corresponds to the continuous longitudinal stiffeners running through the diaphragms in practical applications, as shown in Fig. 13(a).

Case II – The uniform compressive displacements were only applied on the plate, indicating that the longitudinal stiffeners are not directly loaded. This case corresponds to the discontinuous longitudinal stiffeners broken by the diaphragms in practical applications, as shown in Fig. 13(b).
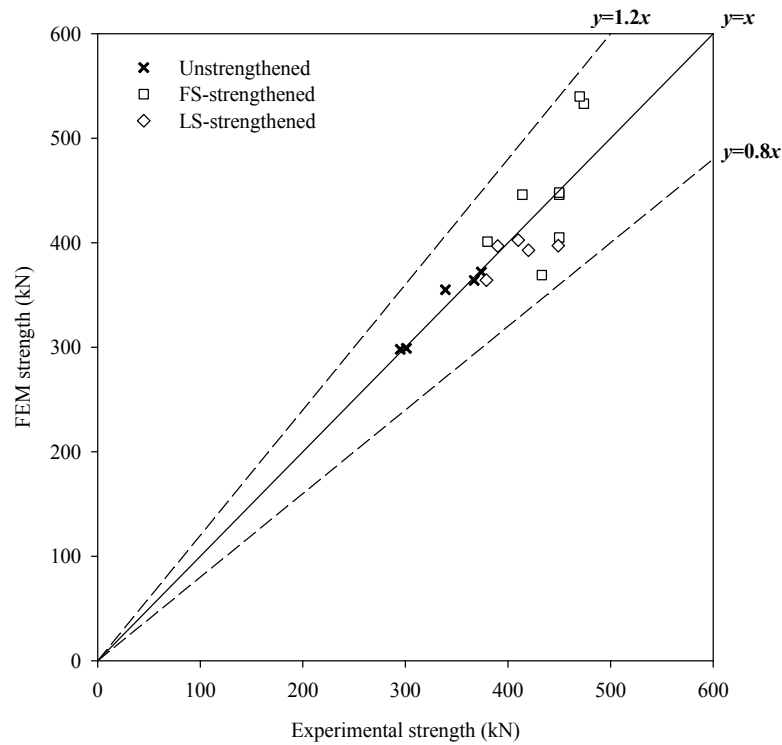
4.2 FEM validation

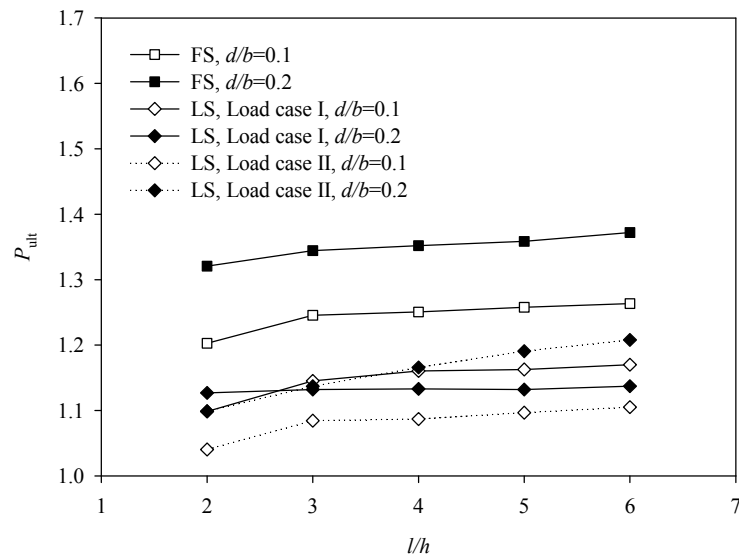Fig. 14 Comparison of experimental strengths and FEM results

Fig. 15 Variation of strength enhancement factor as a function of plate aspect ratio
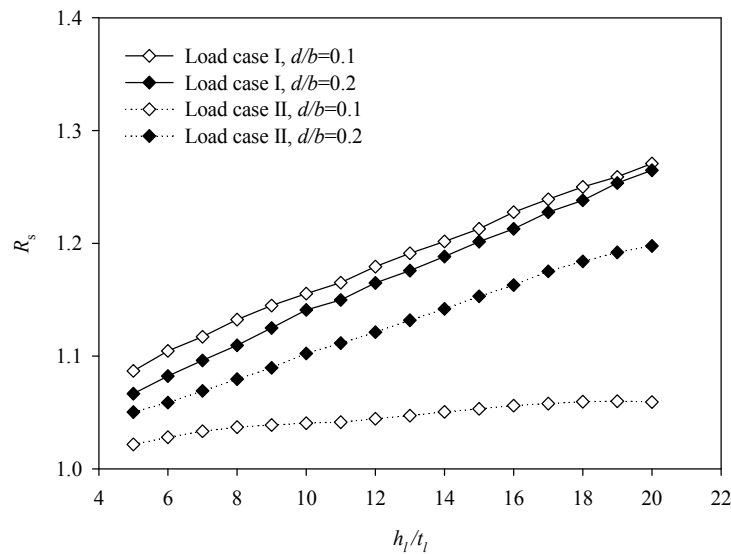

Fig. 16 Variation of strength enhancement factor as a function of stiffener slenderness ratio

A mesh sensitivity study was first carried out for the plates with varying dimensions. The FE meshes produced by the selected mesh-controlling parameters were compared to those of half-size refined meshes. Results indicate that the ultimate strength differences were less than 1%. Furthermore, the FEM results were also compared with the test data, as plotted in Fig. 14. It shows that numerical results coincide with experimental strengths very well, with the averaged values of absolute errors equal to 5.6%. Therefore, the selected mesh-controlling parameters could be considered as accurate enough for the research.
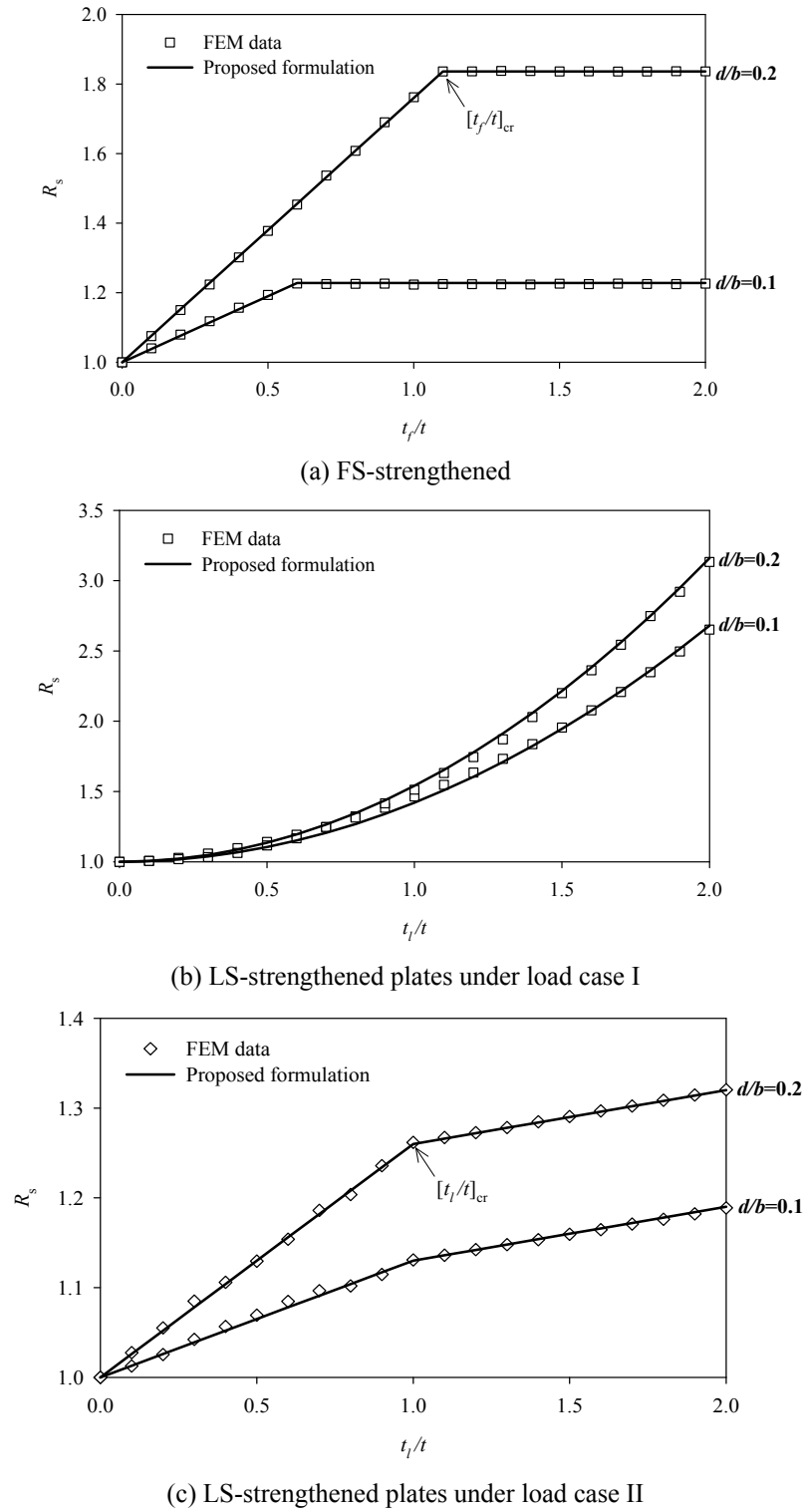
Bin Cheng, Jie Wu and Jianlei Wang

(a) FS-strengthened

(b) LS-strengthened plates under load case I

(c) LS-strengthened plates under load case II

Fig. 17 Variation of strength enhancement factor as a function of stiffener thickness

4.3 FEM analysis results

4.3.1 Influence of hole spacing

Taking the cases of four holes as examples, the infulences of hole spacing (l/h) on ultimate strength (P_{ult}) were studied by changing the plate aspect ratios. It can be seen from Fig. 15 that the variations of ultimate strength with hole spacing are totally invisible, with R_s of $l/h = 2$ being slightly smaller than the others. Therefore, the hole spacing as well as the plate aspect ratio are expected to have ignorable impact on the plate's bearing capacity and thus could be more flexibly determined by considering other practical conditions rather than structural safety. Commonly, hole spacings no small than 3 times the hole lengths ($l/h \geq 3$) are suggested.

4.3.2 Influence of stiffener slenderness ratio

Fig. 16 shows the influences of stiffener slenderness ratio (h_l/t_l) on ultimate strength (P_{ult}) of LS-strengthened plates. It can be seen that P_{ult} of both load cases are appropriate linearly enhanced by increasing h_l/t_l from 5 to 20, with the increasing rates of load case II curves being smaller than those of load case I. It suggests that an increase in the slenderness ratio of the longitudinal stiffener is always beneficial for the improvements of compression strength, since both compression area and lateral stiffness of perforated plates have been constantly enhanced. However, the slenderness ratio of a stiffener is commonly required in AASHTO (2005) and Eurocode 3 (2006) to be not too large, since slender stiffeners are more prone to local buckling under compression. Therefore, slenderness ratio of 10 is recommended for the longitudinal stiffeners and will be adopted in the following analyses.

4.3.3 Influence of stiffener thickness

Fig. 17 shows the influences of stiffener thickness (t_f, t_l) on ultimate strength improvement factor (R_s) of strengthened plates with $d/b = 0.1$ and 0.2. It can be seen that R_s of FS-strengthened plate first increases linearly and then keeps constant as t_f/t is increased from 0 to 2. A critical stiffener thickness/plate thickness, i.e., $[t_f/t]_{cr}$ in Fig. 17, exists in each case. Inflection points are also evident for the LS-strengthened plates under load case II, while R_s keeps increasing slightly with increasing t_l/t when t_l/t is greater than $[t_l/t]_{cr}$. The reason lies in that an increase in the dimension of longitudinal stiffener always provides significant improvement in the moment inertia of the plate cross-section, which is considered as the most important for the bearing capacity of an axially compressed plate which fails according to overall deformation mode, see LS-strengthened specimens in Fig. 8. While for the LS-strengthened plates under load case I, i.e., uniform displacements were applied both on the plate and the stiffeners, R_s is always quadratically promoted by increasing the stiffener thickness since the cross-section area of the stiffener, as used to bear the compression loads directly, is proportional to the square of its thickness. Therefore, continuous longitudinal stiffeners running across the diaphragms, as shown in Fig. 13(a), should be recommended in engineering applications.

By employing the stiffener thickness as variable and using numerical fitting method, the following simplified formulas are proposed for the ultimate strength estimation of integral FS-strengthened and LS-strengthened plates under uniaxial compression.

For integral FS-strengthened plates

$$R_s = k_f \cdot (t_f/t) + 1 \quad \text{for} \quad t_f/t \leq [t_f/t]_{cr}, \quad \text{or}$$

$$R_s = R_{fu} \quad \quad \text{for} \quad t_f/t \geq [t_f/t]_{cr}$$

where $[t_f / t]_{cr} = 5 \cdot (d/b) + 0.1$

$$k_f = 3.8 \cdot (d/b)$$

$$R_{fu} = 19 \cdot (d/b)^2 + 0.38 \cdot (d/b) + 1$$

For LS-strengthened plates under load case I:

$$R_s = k_l \cdot (t_l / t)^2 + 1$$

$$\text{where} \quad k_{l,1} = 1.2 \cdot (d/b) + 0.3$$

For LS-strengthened plates under load case II:

$$R_s = k_{l,1} \cdot (t_l / t) + 1 \qquad \text{for} \quad t_l / t \le [t_l / t]_{cr} \quad \text{or}$$

$$R_s = k_{l,2} \cdot (t_l / t) + R_{lu} \quad \text{for} \quad t_l / t \ge [t_l / t]_{cr}$$

where $[t_l / t]_{cr} = 1.0$

$$k_{l,1} = 1.3 \cdot (d/b)$$

$$k_{l,2} = 0.06$$

$$R_{lu} = 1.3 \cdot (d/b) + 0.94$$

The fitting curves, as ploted in Fig. 17, match the numerical data points very well. By further introducing the strength formulation of unstrengthened plates provided by Cheng *et al.* (2013a), the ultmate compression strengths of strengthened plates containing continuous elliptical holes can be written as

$$P_{ult} = R_s \cdot \left(1.05 - 2 \cdot \frac{d}{b} \right) \cdot S_y \cdot b \cdot t$$

where S_y is the yield stress of steel. Note that the proposed formulas can be used only for the situations of $b/t \le 30$, $l/h \ge 3$, $0.1 \le d/b \le 0.2$, and $h_f / t_f = h_l / t_l = 10$.

4.3.4 Comparison of strengthening efficiency

Strengthening efficiencies of two types of stiffeners were further investigated by employing the relative weight of stiffener (w_f and w_l). Here, the relative weight of stiffener is defined as the weight ratio of strengthening stiffener to strengthened plate, and can be calculated as

$$w_f = \frac{b_f \cdot t_f \cdot a_f}{b \cdot t \cdot a} \quad \text{for FS-strengthened plates, and}$$

$$w_f = \frac{h_l \cdot t_l}{b \cdot t} \quad \text{for LS-strengthened plates.}$$

Fig. 18 shows the variations of ultimate strength (P_{ult}) as well as its improvement factors (R_s)

with relative weight of stiffener (w_f, w_l), where higher curves represent better efficiencies. Conclusion can be made as follows:

(1) For the hole sizes discussed (i.e., $d/b = 0.1$ and 0.2), LS curves of load case I, where linear relationships between R_s and w_l are evident, are always located above the FS curves, indicating that the continuous longitudinal stiffener provides higher strengthening efficiency than the flat stiffener.

(2) Intersections between LS curves of load case II and FS curves are commonly observed. In most occasions, flat stiffeners behave better strengthening efficiencies than discontinuous longitudinal stiffeners. The latter can only be preferred if the required strength improvement is relatively small, as shown in the shadow area of Fig. 18.

(3) Similarly, discontinuous longitudinal stiffeners can hardly provide higher strengthening efficiencies than continuous ones, since the curve slopes of load case II are significantly smaller than those of load case I in most occasions.

Generally speaking, continuous longitudinal stiffeners that participate in the compression bearing should be preferred for the cutout-strengthening of plates containing double-row continuous elliptical holes, followed by flat stiffeners. The longitudinal stiffeners used for strengthening should not be broken by diaphragms or others, especially when the ultimate strengths of perforated plates need to be substantially improved.

5. Conclusions

This paper focuses on the cutout-strengthening method used for improving the compression strengths of perforated plates containing double-row continuous elliptical holes. The following conclusions can be made:

(1) The stress concentrations near the hole edge were more or less depressed by the stiffeners considered, and the longitudinal stiffeners could be more efficient than the flat stiffeners in reducing SCF values.

(2) The flat stiffeners are helpless in preventing the steels near the hole edge from locally buckling, and the regions between adjacent separated flat stiffeners are more prone to deform remarkably in ultimate states. Overall failure patterns are commonly observed for the plates strengthened by longitudinal stiffeners.

(3) The integral flat stiffeners are more effective in enhancing the bearing capacities of perforated plates when compared to the separated flat stiffeners, and the strength improvements due to integral flat stiffeners are also higher than those of longitudinal stiffeners in case of identical stiffener thicknesses.

(4) The influences of hole spacing as well as plate aspect ratio on the ultimate strengths of strengthened plates are totally invisible.

(5) An increase in the slenderness ratio of longitudinal stiffener is always beneficial for the improvements of compression strength. However, slenderness ratio of 10 is recommended due to probable local buckling of slender stiffeners.

(6) As the stiffener becomes thicker, the ultimate strengths of FS-strengthened plates increase linearly and then keep constant when the stiffener thickness exceeds a critical value. For the LS-strengthened plates whose longitudinal stiffeners are free of direct compressions (i.e., discontinuous longitudinal stiffeners), slight improvements of ultimate strength with

increasing stiffener thickness are observed when the stiffener thicknesses are greater than the critical value. While for the LS-strengthened plates where compressions are applied on both the plate and the stiffeners (i.e., continuous longitudinal stiffeners), the ultimate strengths are always quadratically promoted by the increasing stiffener thickness.

(7) Strengthening efficiency analysis indicates that, in most occasions, the continuous longitudinal stiffeners are of the most efficient in strengthening the plates perforated by continuous elliptical holes, followed by the flat stiffeners. The longitudinal stiffeners used for strengthening should not be broken by the diaphragms or others, especially when the ultimate strengths of perforated plates need to be substantially improved.

(8) The simplified formulas used for predicting the compression strengths of strengthened plates are proposed on the basis of numerical fitting of parametric analysis results.

Acknowledgments

References

AASHTO LRFD Bridge design specifications (2013), American Association of State Highway and Transportation Officials, (6th Edition), 2013 interim revisions.

ANSYS 12 [Computer software] (2009), Ansys Inc., Canonsburg, PA, USA.

Azizian, Z.G. and Roberts, T.M. (1983), "Buckling and elasto-plastic collapse of perforated plates", *Proceedings of the International Conference on Instability and Plastic Collapse of Steel Structures*, London, UK, August.

Cheng, B. and Li, C. (2012), "Buckling behavior of strengthened perforated plates under shear loading", *Steel Compos. Struct., Int. J.*, **13**(4), 367-382.

Cheng, B. and Zhao, J. (2010), "Strengthening of perforated plates under uniaxial compression: Buckling analysis", *Thin-Wall. Struct.*, **48**(12), 905-914.

Cheng, B., Wang, J. and Li, C. (2013a), "Compression behavior of perforated plates in steel tower anchorage zones of cable-stayed bridges", *J. Constr. Steel Res.*, **90**, 72-84.

Cheng, B., Wang, J. and Li, C. (2013b), "Compression tests and numerical analysis of perforated plates containing slotted holes in steel pylons", *Thin-Wall. Struct.*, **67**, 129-143.

El-Sawy, K.M., Nazmy, A.S. and Martini, M.I. (2004), "Elasto-plastic buckling of perforated plates under uniaxial compression", *Thin-Wall. Struct.*, **42**(8), 1083-1101.

Eurocode 3 (2006), Design of steel structures, Steel bridge, British Standards Institution; BS EN 1993-2: 2006.

Li, F., He, Y.T., Fan, C.H., Li, H.P. and Zhang, H.X. (2008), "Investigation on three-dimensional stress concentration of LY12-CZ plate with two equal circular holes under tension", *Mater. Sci. Eng.*, **483-484**, 474-476.

Maiorana, E., Pellegrino, C. and Modena, C. (2008), "Linear buckling analysis of perforated plates subjected to localized symmetrical load", *Eng. Struct.*, **30**, 3151-3158.

Maiorana, E., Pellegrino, C. and Modena, C. (2009), "Non-linear analysis of perforated steel plates subjected to localized symmetrical load", *J. Constr. Steel Res.*, **65**, 959-964.

Moen, C.D. and Schafer, B.W. (2009), "Elastic buckling of thin plates with holes in compression or

bending", *Thin-Wall. Struct.*, **47**(12), 1597-1607.

Muskhelishvili, N.I. (1963), Some basic problems of the mathematical theory of elasticity, Springer, Groningen, Netherlands.

Narayanan, R. and Chow, F.Y. (1984), "Ultimate capacity of uniaxially compressed perforated plates", *Thin-Wall. Struct.*, **2**(3), 241-264.

Narayanan, R. and Rockey, K.C. (1981), "Ultimate load capacity of plate girders with webs containing circular cut-outs", *Proceedings of Institution of Civil Engineers*, **71**(3), 845-862.

Paik, J.K. (2007a), "Ultimate strength of perforated steel plates under edge shear loading", *Thin-Wall. Struct.*, **45**(3), 301-306.

Paik, J.K. (2007b), "Ultimate strength of steel plates with a single circular hole under axial compressive loading along short edges", *Ships Offshore Struct.*, **2**(4), 355-360.

Paik, J.K. (2008), "Ultimate strength of perforated steel plates under combined biaxial compression and edge shear loads", *Thin-Wall. Struct.*, **46**(2), 207-213.

Peterson, R.E. (1974), *Stress Concentration Factor*, John Wiley and Sons, New York, NY, USA.

Savin, G.N. (1961), *Stress Concentration around Holes*, Pergamon Press, New York, NY, USA.

Shanmugam, N.E., Thevendran, V. and Tan, Y.H. (1999), "Design formula for axially compressed perforated plates", *Thin-Wall. Struct.*, **34**(1), 1-20.

She, C.M. and Guo, W.L. (2007), "Three-dimensional stress concentrations at elliptic holes in elastic isotropic plates subjected to tensile stress", *Int. J. Fatigue*, **29**(2), 330-335.

Yang, Z., Kim, C.B., Cho, C. and Beom, H.G. (2008), "The concentration of stress and strain in finite thickness elastic plate containing a circular hole", *Int. J. Solid. Struct.*, **45**(3-4), 713-731.

Yu, P.S., Guo, W.L., She, C.M. and Zhao, J.H. (2008), "The influence of Poisson's ratio on thickness-dependent stress concentration at elliptic holes in elastic plates", *Int. J. Fatigue*, **30**(1), 165-171.

CC